frontiers in Materials

MINI REVIEW
published: 16 November 2020
doi: 10.3389/fmats.2020.594771

Spin-Orbit Torques in Transition Metal Dichalcogenide/Ferromagnet Heterostructures

Jan Hidding and Marcos H. D. Guimarães**

Zernike Institute for Advanced Materials, University of Groningen, Groningen, Netherlands

In recent years, there has been a growing interest in spin-orbit torques (SOTs) for manipulating the magnetization in nonvolatile magnetic memory devices. SOTs rely on the spin-orbit coupling of a nonmagnetic material coupled to a ferromagnetic layer to convert an applied charge current into a torque on the magnetization of the ferromagnet (FM). Transition metal dichalcogenides (TMDs) are promising candidates for generating these torques with both high charge-to-spin conversion ratios, and symmetries and directions which are efficient for magnetization manipulation. Moreover, TMDs offer a wide range of attractive properties, such as large spin-orbit coupling, high crystalline quality and diverse crystalline symmetries. Although numerous studies were published on SOTs using TMD/FM heterostructures, we lack clear understanding of the observed SOT symmetries, directions, and strengths. In order to shine some light on the differences and similarities among the works in literature, in this mini-review we compare the results for various TMD/FM devices, highlighting the experimental techniques used to fabricate the devices and to quantify the SOTs, discussing their potential effect on the interface quality and resulting SOTs. This enables us to both identify the impact of particular fabrication steps on the observed SOT symmetries and directions, and give suggestions for their underlying microscopic mechanisms. Furthermore, we highlight recent progress of the theoretical work on SOTs using TMD heterostructures and propose future research directions.

Keywords: spin-orbit torques (SOT), transition metal dichalcogenides (TMD), van der Waals materials, spin-orbitronics, Two-dimensional materials (2D materials)

OPEN ACCESS

Edited by:
Myung Gwan Hahm,
Inha University, South Korea

Reviewed by:
Bipin Kumar Gupta,
National Physical Laboratory (CSIR), India
Narayanan Tharangattu Narayanan,
Tata Institute of Fundamental Research, India

****Correspondence:***
Marcos H. D. Guimarães
m.h.guimaraes@rug.nl
Jan Hidding
jan.hidding@rug.nl

Specialty section:
This article was submitted to Quantum Materials, a section of the journal Frontiers in Materials

Received: *14 August 2020*
Accepted: *12 October 2020*
Published: *16 November 2020*

Citation:
Hidding J and Guimarães MHD (2020) Spin-Orbit Torques in Transition Metal Dichalcogenide/Ferromagnet Heterostructures. Front. Mater. 7:594771. doi: 10.3389/fmats.2020.594771

INTRODUCTION

Spin-orbit torques (SOTs) are promising candidates for effective manipulation of magnetization through electric currents with applications in nonvolatile magnetic memory and logic devices. SOTs convert an electric current into a magnetic torque in non-magnetic/ferromagnetic heterostructure, i.e., an electric current through the stack can modulate the direction of the ferromagnet's magnetization (Gambardella and Miron, 2011; Manchon et al., 2019). Devices showing large SOT efficiencies usually rely on a nonmagnetic material with large spin-orbit coupling in contact with a ferromagnet (FM). Transition metal dichalcogenides (TMDs), with chemical formula MX_2, where M is a transition metal (e.g., Mo, and W) and X a chalcogen element (e.g., S and Se), can provide large spin-orbit coupling and pristine surfaces which can result in a more intimate contact between the TMD and the FM layer. Furthermore, this family of materials offers a wide range of electronic and crystalline properties and symmetries. Although numerous articles were

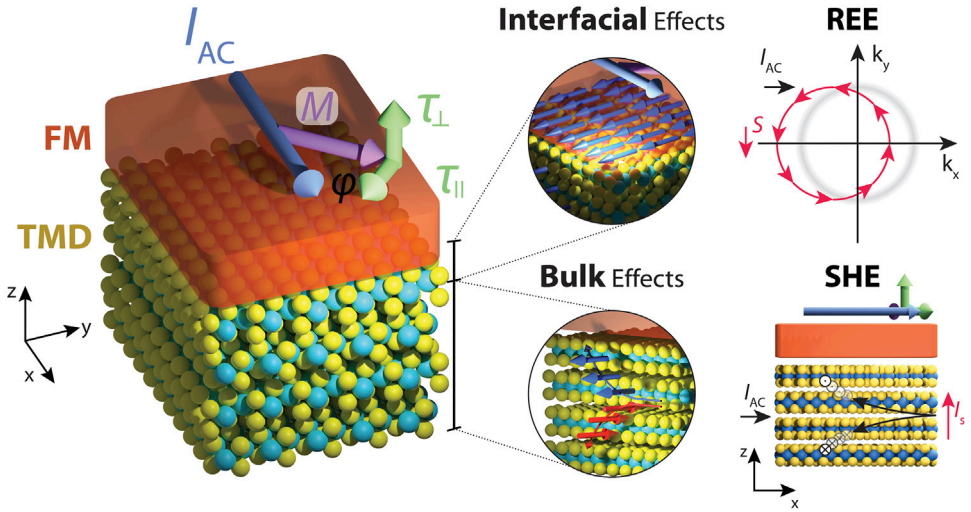

FIGURE 1 | Schematics of SOTs in TMD/FM heterostructures. A charge current, usually oscillating at low (RF) frequencies for SHH (ST-FMR) measurements is applied along a device consisting of a TMD layer and a FM. The magnetization of the FM layer, oriented along an external magnetic field, observes a current-induced SOT in-plane ($\tau_{\parallel}$) and out-of-plane ($\tau_{\perp}$), indicated by the green arrows. These torques may arise from multiple microscopic effects arising in the bilayer, which may originate either from the TMD/FM interface (top), e.g., through the Rashba-Edelstein Effect (REE), or the bulk of the material (bottom), as for example through a spin Hall effect (SHE) in the TMD layer.

published on SOTs in TMD/ferromagnetic heterostructures, a clear understanding of the different mechanisms underlying observed SOTs remain yet to be understood.

In this mini-review, we give an overview of the recent progress on SOTs in TMD/FM heterostructures. Materials with high charge-to-spin conversion efficiencies, such as WTe_2 and $TaTe_2$ (Safeer et al., 2019; Zhao et al., 2020; Hoque et al., 2020), are often considered as good candidates for large SOT efficiencies. However, large charge-to-spin conversion efficiencies are no guarantee for large SOT efficiencies, as SOTs are often an emergent phenomenon, depending on proximity effects (spin-orbit coupling and magnetic exchange), wavefunction overlap, and interface spin transparency (spin mixing conductance) as well. Indeed, the observed torques in TMD/FM heterostructures cannot always be explained by well-known effects such as the bulk spin Hall effect (SHE) (Dyakonov and Perel, 1971; Hirsch, 1999; Sinova et al., 2015) or the interfacial Rashba-Edelstein Effect (REE) (Edelstein, 1990; Ganichev et al., 2002; Kato et al., 2004; Mihai Miron et al., 2010; Ganichev et al., 2016) (**Figure 1**), indicating that other mechanisms involving material specific properties or interfacial effects are into play. This is supported by recent works suggesting that both the type of ferromagnetic layer (Dolui and Nikolic, 2020; Go and Lee, 2020) and the interface properties between the TMD and the ferromagnetic layer (Amin et al., 2020; Sousa et al., 2020; Go et al., 2020) (Sahoo et al., 2020; Kumar et al., 2020; Xue et al. 2020) are of paramount importance for the observed SOTs, allowing for enhanced and unconventional SOTs.

To describe to different torques, we use the notation in terms of odd ($\tau_o^{\zeta} \propto \hat{m} \times \hat{\zeta}$) or even ($\tau_e^{\zeta} \propto \hat{m} \times (\hat{\zeta} \times \hat{m})$) with respect to the magnetization direction ($\hat{m}$), with $\zeta = x, y, z$. These torques are also named, respectively, field-like (FL) and damping-like (DL) torques in many papers in literature (Manchon et al., 2019), with directions out-of-plane or in-plane with respect to the TMD/FM plane (**Figure 1**). For a fair comparison between the results in literature we use the torque conductivities ($\sigma_{o(e)}^{\zeta}$) to quantify the SOT strength, which expresses the torques per unit area per unit electric field. This figure of merit is adopted rather than the torque efficiency ($\xi_{FL(AD)}^{j_c}$), because the electric field across the device can be more accurately determined when compared to the current density (Nguyen et al., 2016).

DISCUSSION ON RECENT PROGRESS

The field of SOTs using TMD-based devices has been rapidly developed in the past 5 years. Experimental studies have used different TMD sources (e.g., mechanical exfoliation or chemical vapor deposition, CVD), FM materials, deposition methods (e.g., sputtering or electron-beam evaporation), and measurement techniques, namely second-harmonic Hall (SHH) (Garello et al., 2013; Hayashi et al., 2014; Avci et al., 2014; Ghosh et al., 2017) or spin-torque ferromagnetic resonance (ST-FMR) (Liu et al., 2011; Fang et al., 2011; Berger et al., 2018). So far, it is unclear how these different techniques and procedures affect the measured SOTs.

In this section, we discuss the results for semiconducting, semi-metallic and metallic TMDs, giving an overview of their fabrication and measurement techniques (**Table 1**). Comparing the TMDs in this way allows us to pinpoint important differences and similarities in the observed torques.

Semi-Conducting TMDs

Shao *et al.* were one of the first to examine SOTs in TMD/FM heterostructures (Shao et al., 2016). There, SOTs were quantified

TABLE 1 | Recent studies on TMD/FM heterostructures with their fabrication techniques and spin torque conductivities.

Reference	SOT material (thickness)	Fabrication technique	Ferro-magnet	Deposition technique	Measurement technique	Spin torque conductivity [$\times 10^3 (\hbar/2e)(\Omega m)^{-1}$]	Proposed mechanism/ Source
	Semiconducting						
(Shao et al., 2016)	MoS_2 (1 L)	CVD	CoFeB (3 nm)	Magnetron sputtering	SHH	$\sigma_o^y = 2.88$	REE
(Shao et al., 2016)	WeS_2 (1 L)	CVD	CoFeB (3 nm)	Magnetron sputtering	SHH	$\sigma_o^y = 5.52$	REE
(Zhang et al., 2016)	MoS_2 (1 L)	CVD	Py (5 nm)	Magnetron sputtering	ST-FMR	σ_e^y =Observed	Interfacial
(Lv et al., 2018)	WS_2 (1 L)	CVD	Py (10 nm)	E-beam evaporation	ST-FMR	σ_o^y =Observed	REE
						σ_e^y =Observed	REE
	Semi-metallic						
(MacNeill et al., 2017a)	WTe_2 (1.8–15 nm)	Exfoliation	Py (6 nm)	Sputtering	ST-FMR/SHH	$\sigma_o^y = 9 \pm 3$	Interfacial
						$\sigma_e^y = 8 \pm 2$	Interfacial
						$\sigma_e^z = 3.6 \pm 0.8$	Interfacial
						$\sigma_o^z = 0$	-
(MacNeill et al., 2017b)	WTe_2 (1 L–16 nm)	Exfoliation	Py (6 nm)	Sputtering	ST-FMR/SHH	σ_o^y =Observed	Oersted
						σ_e^y =Observed	-
						σ_e^z =Observed	-
						$\sigma_o^z = 0$	-
(Li et al., 2018)	WTe_2 (5.6–31 nm)	Exfoliation	Py (6 nm)	Sputtering	SHH	$\sigma_o^y = 1.3 \times 10^2$	Fermi arcs
						σ_e^y =Observed	-
(Shi et al., 2019)	WTe_2 (5.8–122 nm)	Exfoliation	Py (6 nm)	Sputtering	ST-FMR/SHH	$\sigma_e^y = 6 \times 10^1$(l//b)	
						$\sigma_e^y = 5.95$ (l//a)	Bulk
						σ_e^z =Observed (l//a)	
(Stiehl et al., 2019b)	$TaTe_2$ (4.5–19.7 nm)	Exfoliation	Py (6 nm)	Sputtering	ST-FMR/SHH	σ_e^y =Weak	-
						σ_o^z =Sometimes observed	-
						$\sigma_e^z = 0$	-
						σ_o^x =Observed (Dresselhaus)	Oersted (resist. anisotropy)
(Stiehl et al., 2019a)	$MoTe_2$ (1 L–14.2 nm)	Exfoliation	Py (6 nm)	Sputtering	ST-FMR	$\sigma_o^y = 15$	Oersted
						$\sigma_e^y = 5.8 \pm 0.16$	Interfacial
						$\sigma_e^z = 1.02 \pm 0.03$	Interfacial
						$\sigma_o^z = 0.81 \pm 0.05$(t > 3 nm)	Interfacial
(Xu et al., 2020)	$PtTe_2$ (3–20 nm)	CVD	Py (2.5, 5.0, 7.5, 10 nm)	Sputtering	ST-FMR	σ_o^y =Observed	-
						$\sigma_e^y = 1.6 \times 10^2$	SHE + TSS
	Metallic						
(Guimarães et al., 2018)	$NbSe_2$ (1–10 L)	Exfoliation	Py (6 nm)	Sputtering	ST-FMR	$\sigma_o^y = 40$	Oersted
						$\sigma_e^y = 3$	REE
						$\sigma_e^z = 0$	-
						$\sigma_o^z = 1$	Strain
(Husain et al., 2020)	1T-TaS_2 (1 L)	Ion-beam sputtering	Py	-	ST-FMR/SHH	σ_o^y =Negligible	-
						$\sigma_e^y = 2.63 \times 10^2$	Interfacial

by the non-resonant SHH measurements on monolayer (1L) MoS_2 and WSe_2 coupled with CoFeB (3 nm). They observed a temperature independent out-of-plane FL torque τ_o^y $(\hat{m} \times \hat{y})$ for both devices with a corresponding torque conductivity of $\sigma_o^y = 2.88 \times 10^3\,(\hbar/2e)\,(\Omega m)^{-1}$ and $5.52 \times 10^3\,(\hbar/2e)\,(\Omega m)^{-1}$ for MoS_2 and WSe_2, respectively. No in-plane DL torque of the form τ_e^y $(\hat{m} \times (\hat{y} \times \hat{m}))$ was observed in either of their devices. This DL torque is observed in SOT measurements on Pt/Py bilayers and is often ascribed to the SHE (Ramaswamy et al., 2018). Since the monolayer TMDs are much less conductive than the FM layer, the SOTs here are interfacial in nature, and the results point to the REE mechanism (Miron et al., 2011; Haney et al., 2013; Amin and Stiles, 2016a; Amin and Stiles, 2016b).

Interestingly, in a concurrent work, Zhang *et al.* obtained different results using a high-frequency technique, ST-FMR, on 1L-MoS_2/Permalloy ($Ni_{80}Fe_{20}$ – Py) 5 nm (Zhang et al., 2016). There, they identified an in-plane DL τ_e^y $(\hat{m} \times (\hat{y} \times \hat{m}))$ and an out-of-plane FL torque τ_o^y $(\hat{m} \times \hat{y})$. A torque ratio, $\tau_o^y/\tau_e^y = 0.19 \pm 0.01$ was obtained, indicating that τ_e^ydominates over τ_o^y, in contrast to the results by Shao and co-workers. This result was repeated using different deposition techniques of the FM layer (sputtering or electron-beam deposition), indicating that the observed torque is independent on the Py deposition technique. The different measurement techniques used by the two groups could explain the discrepancy in the observed torques. However, it has been shown that the SOTs quantified by ST-FMR and SHH techniques agree within the experimental accuracy for several systems (MacNeill et al., 2017a; MacNeill et al., 2017b; Stiehl et al., 2019b; Shi et al., 2019).

The discrepancy between results for MoS_2/FM bilayers suggests that not only the spin-orbit material but also the type of ferromagnetic material (CoFeB vs Py) can play a significant role in the observed torques. This is theoretically substantiated in a recent work (Dolui and Nikolic, 2020), where calculations on $MoSe_2$/Co, WSe_2/Co and $TaSe_2$/Co heterostructures were performed. They find that the hybridization of the Co wavefunctions with those of the TMDs leads to dramatic transmutation of the electronic and spin structure of the Co layers, even within eight layers away from the interface. This suggests that injecting unpolarized spin currents in these spin-orbit-proximitized layers of Co generates nonequilibrium spin densities, which in turn leads to a nonzero local torque on the magnetization. Both the spin polarization direction and magnitude were shown to differ between the different TMDs and complex spin textures were obtained for the spin-orbit-proximitized layers. These results indicate that the FM material can play an active role in the type of SOTs observed. Moreover, recent theoretical works (Sousa et al., 2020) pointed out that different scattering mechanisms lead to different torque symmetries, indicating that the sample quality, symmetry and nature of scatterers also plays a role here. Different FM materials in FM/TMD heterostructures might therefore exhibit different SOTs as was the case for Shao *et al.* and Zhang *et al.*

More recently, WS_2 was studied by Lv *et al.* in a 1L-WS_2/Py (10 nm) heterostructure (Lv et al., 2018) using CVD-grown WS_2 and electron-beam evaporated Py layer. The authors observe both a DL torque τ_e^y and a FL torque τ_o^y in their ST-FMR measurements, which are ascribed to the interfacial REE. Furthermore, they observed a gate-dependent SOT ratio ranging from $\tau_o^y/\tau_e^y = 0.05$ to 0.22 within a range of $V_g = -60$ V to 60 V, absent in their reference sample of Pt/Py. Gate-dependent SOTs were observed in SHH measurements on a topological insulator (Fan et al., 2016), but not yet reported in TMD/FM heterostructures. The increasing SOT ratio with gate-voltage could be explained by an increased carrier density leading to an enhanced current at the WS_2/Py interface. The modulation of SOT strength using a gate voltage is a step toward applications for data storage and processing and more research should be done to improve the gate tunability of SOTs in TMD/FM heterostructures (Li et al., 2020; Filianina et al., 2020; Dieny et al., 2019).

Semi-Metallic TMDs

In addition to semiconducting TMDs, a variety of semi-metallic TMDs have been studied, with special focus given to low-symmetry crystals. A particularly interesting candidate is WTe_2, belonging to space group $Pmn2_1$. In a WTe_2/FM heterostructure, however, the symmetries are reduced to a single mirror plane perpendicular to the a-axis and the identity, space group *Pm*. The low device symmetry allows for unconventional SOTs, such as an out-of-plane DL torque τ_e^z $(\hat{m} \times (\hat{z} \times \hat{m}))$, which is especially interesting for applications in high-density memory devices since these torques are very effective for magnetization switching of perpendicular magnetic anisotropy materials (Ramaswamy et al., 2018).

MacNeill *et al.* were the first to examine SOTs using WTe_2 (MacNeill et al., 2017a). Using ST-FMR, the authors observed τ_e^z, along the conventional SOTs τ_o^y and τ_e^y, and extracted a torque conductivity of $\sigma_e^z = 3.6 \pm 0.8 \times 10^3\ (\hbar/2e)\,(\Omega m)^{-1}$ with the current driven along the low-symmetry a-axis. The other FL and DL torque conductivities were measured at $\sigma_o^y = 9 \pm 3 \times 10^3\ (\hbar/2e)\,(\Omega m)^{-1}$ and $\sigma_e^y = 8 \pm 2 \times 10^3\ (\hbar/2e)\,(\Omega m)^{-1}$, respectively. The magnitude of τ_e^z was found to depend on the angle between the electric current and the WTe_2 a-axis, showing a gradual decrease of the torque ratio τ_e^z/τ_o^y when the projection of the current on the b-axis increases, giving support to its origin being correlated with the crystal symmetry. Even though an initial thickness dependence on the torques revealed little variation, a more thorough study with a wider thickness range ($t = 0.7 - 16$ nm) revealed additional bulk contributions to the SOTs in addition to the interfacial ones (MacNeill et al., 2017b). The thickness dependence of $|\tau_o^y|$, shows a strong increase with increasing WTe_2 thickness, suggesting it originates from an Oersted field produced by the current in the WTe_2 layer. The unusual out-of-plane DL torque τ_e^z shows a slowly decreasing magnitude with increasing thickness ($t \geq 4$ nm), while thinner layers show significant device-to-device variations. In the same work, the authors indicated that the in-plane DL torque τ_e^y possesses a similar thickness dependence as τ_e^z. These torques remain large down a WTe_2 monolayer, suggesting that their microscopic origin is interfacial with some possible (smaller) additional bulk contribution.

Subsequent studies indicated a strong temperature dependence (2 – 300 K) on τ_o^y with the current flowing along the b-axis of WTe_2 using ST-FMR measurements (Li et al., 2018). While this temperature dependence was observed for thicker samples (20 and 31 nm), thinner samples (5.6 and 7.0 nm) only showed a weak temperature dependence. Furthermore, for a current applied along the a-axis (I//a), no temperature dependence is observed. A torque conductivity as high as $\sigma_o^y = 1.3 \times 10^5\ (\hbar/2e)\,(\Omega m)^{-1}$was reported. Calculations of the Oersted field contribution to τ_o^y could not explain the large enhancement. The enhanced SOT at low temperatures with I//b-axis was therefore ascribed to a spin accumulation created by spin-momentum locking in Fermi arcs which exist only along the b-axis, experimentally observed for WTe_2 nanoribbons with thicknesses in the range of 10–40 nm (Li et al., 2017). The origin of the relatively high τ_o^y which remains for thinner devices, is ascribed to the REE.

More recently, WTe_2/Py heterostructures have been shown to be very efficient for current-induced in-plane magnetization switching, with switching current densities in the order of 10^5 A/cm^2 (Shi et al., 2019). In the same work, the authors also reported a thickness dependence on the spin Hall efficiency in WTe_2, with larger values at higher thicknesses. However, the ST-FMR results show a significant frequency dependence and the role of artifacts such as skin-depth effects could not be ruled out. Nevertheless, the low threshold for current-induced magnetization switching indicates a promising direction for TMDs in future applications. Interestingly, these structures have also shown the presence of a Dzyaloshinskii-Moriya interaction, an essential ingredient for chiral magnetism.

The anisotropic in-plane conductivity in low-symmetry crystals can also impact SOTs. Results on $TaTe_2$/Py heterostructures have shown SOTs with Dresselhaus-like symmetries ($\hat{m} \times \hat{x}$) (Stiehl et al., 2019b). These torques have been shown to arise from Oersted-fields, generated by in-plane transverse current components due to conductivity anisotropy of $TaTe_2$. A similar, albeit smaller effect has been shown to be present in WTe_2/Py bilayers. Apart from the regular Oersted torque and Dresselhaus-like torque in the $TaTe_2$/Py heterostructures, the other torques are small or zero. Cross-sectional high-angle annular dark-field scanning transmission electron microscopy (HAADF-STEM) has indicated intermixing at the $TaTe_2$/Py interface which is likely to affect the effective SOTs due to a change in the local electronic environment and the spin mixing conductance of the interface. Interestingly, a change in the SOTs in topological-insulator/ferromagnet devices due to intermixing at the interface has been recently reported (Bonell et al., 2020). Here we point out that in addition to the changes in the SOTs arising from the different electronic structures for devices using different FM layers (e.g., Py, Co, CoFeB), the materials intermixing should also be carefully considered and potentially quantified in order to obtain a more in-depth understanding of the microscopic mechanisms involved.

Interestingly, both $TaTe_2$ and WTe_2 have shown to induce an in-plane magnetic anisotropy on Py, indicating a strong interaction between the semi-metallic TMDs and the FM layer. The anisotropy induced by WTe_2 was shown to be about 10 s of mT and one order of magnitude larger than the one induced by $TaTe_2$. Additionally, the two TMDs induced anisotropy in different directions with respect to their crystal orientations, hinting toward the dependence of the induced magnetic anisotropy and the electronic structure of the TMD.

Another interesting semi-metallic TMD is β-$MoTe_2$ which, different than WTe_2 and similar to $TaTe_2$, possess inversion symmetry in its bulk form. Using β-$MoTe_2$/Py bilayers Stiehl *et al.* observe the presence of an out-of-plane DL torque τ_e^z using ST-FMR measurements (Stiehl et al., 2019a). This is allowed by the inversion symmetry breaking at the β-$MoTe_2$/Py interface and indicates that inversion asymmetry in the bulk is not a strict requirement for τ_e^z to be observed. The authors report a thickness independent torque conductivity of $\sigma_e^z = 1.02 \pm 0.03 \times 10^3\ (\hbar/2e)\,(\Omega m)^{-1}$, 1/3 of the value reported for WTe_2. The standard in-plane DL torque τ_e^y was also observed with $\sigma_e^y = 5.8 \pm 0.16 \times 10^3\ (\hbar/2e)\,(\Omega m)^{-1}$, and showed no apparent thickness dependence. The lack of a thickness dependent on τ_e^z and τ_e^y for both WTe_2 and β-$MoTe_2$, strongly suggests an interfacial origin for these SOTs.

In addition to the out-of-plane DL torque τ_e^z, the low crystal symmetries of WTe_2 and β-$MoTe_2$ also allow for the presence of an in-plane FL torque $\tau_o^z\ (\hat{m} \times \hat{z})$. While this torque was not observed in WTe_2, it was present in β-$MoTe_2$ devices. There, both τ_e^z and τ_o^z have shown similar temperature dependences, but different thickness dependences, hinting toward two microscopic mechanisms for τ_o^z: one related and another unrelated to τ_e^z. However, the physical mechanisms that generate these torques are still unknown.

More recently, $PtTe_2$/Py devices (Xu et al., 2020) have shown a high spin-torque conductivity for the in-plane DL torque $\sigma_e^y = 1.6 \times 10^5\ (\hbar/2e)\,(\Omega m)^{-1}$. This value is one order of magnitude (or larger) than the values encountered in other TMD-based devices and comparable to devices based on heavy-metal or topological-insulators. This large spin-torque conductivity has been ascribed to a combination of the SHE and spin-momentum locking in topological surface states of $PtTe_2$, as previously observed in topological insulators (Mellnik et al., 2014; Wang et al., 2015; Wang et al., 2017; Clark et al., 2018).

Metallic TMDs

Despite offering stronger spin-orbit interaction and higher conductivity, metallic TMDs have received less attention than their semi-metallic and semiconducting counterparts. To date, only two experimental studies have been reported (Guimarães et al., 2018; Husain et al., 2020).

Thickness dependent ST-FMR measurements on $NbSe_2$ (1–10 layers)/Py heterostructures revealed an in-plane DL torque τ_e^y with a torque conductivity ($\sigma_e^y = 3 \times 10^3\ (\hbar/2e)\,(\Omega m)^{-1}$) comparable to other TMD/Py heterostructures and observable down to a monolayer of $NbSe_2$ (Guimarães et al., 2018). Similar to β-$MoTe_2$/Py (Stiehl et al., 2019a), τ_e^y shows only a weak thickness dependence. An out-of-plane FL torque ($\sigma_o^y = 40 \times 10^3\ (\hbar/2e)\,(\Omega m)^{-1}$) was also observed, and attributed to Oersted fields due to their linear scaling with $NbSe_2$ thickness. However, for thin $NbSe_2$ layers, the estimated

Oersted-field contribution overestimates the observed torque magnitude, and, for monolayer $NbSe_2$ a sign change is observed. These observations for τ_e^y and τ_o^y indicate a contribution from interfacial torques.

In addition to the SOTs with conventional symmetries, an in-plane FL torque τ_o^z $(\hat{m} \times \hat{z})$ was observed in some devices. Since the trigonal symmetry of $NbSe_2$ does not allow for their presence, and given the seemly random thickness dependence of τ_o^z, the authors argue that these torques could arise from uncontrollable strain from the fabrication procedure, which reduces the $NbSe_2$ symmetries. Although τ_e^z is subject to the same symmetry constraints, $\tau_e^z = 0$ for all measured devices, which is in contrast to the torques obtained for WTe_2, where $\tau_o^z = 0$, and $\tau_e^z \neq 0$ (MacNeill et al., 2017a; MacNeill et al., 2017b). This indicates that symmetry analysis alone is not sufficient to predict the observed torques in these systems and that other microscopic factors related to, for example, interface quality (Hayashi et al., 2014; Sousa et al., 2020), Berry curvature (Kurebayashi et al., 2014), or local atomic point-group symmetries (Zhang et al., 2014) could play an important role.

A large spin-torque conductivity of $\sigma_e^y = 2.63 \times 10^5 (\hbar/2e)(\Omega m)^{-1}$ has been recently reported for the metallic monolayer TaS_2/Py heterostructures (Husain et al., 2020) using ST-FMR measurements. This result is attributed to a clean interface which is supported by cross-sectional TEM imaging. Using DFT calculations, the authors observe a considerable redistribution of the band structure which they hold accountable for the prominent DL torque.

CONCLUSION

In this review, we have given an overview of the current status of the field of SOTs in TMD/FM heterostructures. A multitude of SOT symmetries, magnitudes and directions were observed, which could not always be explained by well-known effects such as the SHE and REE. Different mechanisms that do not rely on a large spin-orbit coupling, such as anisotropic in-plane conductivity and uniaxial strain, can also play an important role. Additionally, interfacial effects such as spin-orbit filtering, spin-orbit precession and spin-momentum locking in topological surface states may affect the observed torques. In combination with the large torque conductivities obtained at clean interfaces, this suggests that the TMD/FM interface quality is of paramount importance for both the torque magnitude and direction. Lastly, the ferromagnetic layer, often considered to play a passive role, can have a significant effect on the observed SOTs due to changes of the electronic structure and intermixing at the interface. Dzyaloshinskii–Moriya interaction (DMI) has been shown to arise at TMD/FM interfaces demonstrating a strong interaction between these materials (Kumar et al., 2020; Shi et al., 2019; Wu et al., 2020). The large interfacial DMI in these heterostructures could be explored in future devices combining chiral magnetic structures and SOTs.

Although the crystal symmetry allows for a reasonable prediction of the allowed SOTs, a better understanding of the underlying microscopic mechanisms is key in qualitatively explaining the observed SOTs. In this regard, thickness dependent measurements provide a tool to better differentiate bulk effects from interfacial effects. However, as the contributions of different effects are measured all at once, it remains difficult to distinguish the numerous mechanisms underlying the torques with the current experimental techniques. To clarify the role of the ferromagnetic layer, a variety of devices with different FM materials should be fabricated.

Van der Waals heterostructures composed of TMDs, two-dimensional magnetic materials and graphene should allow for the study of SOTs at the ultimate thickness. Due to their small thickness, in addition to possibly reducing the device footprint, atomically-thin materials are more susceptible to external stimuli, such as gate-voltages, strain and illumination. Along these lines, interesting predictions point to the modulation of SOT and magnetization by gate-voltages in these structures (Dolui et al., 2019; Zollner et al., 2020). The exploration of gate-tunable SOTs in TMD/FM heterostructures could serve as a first step toward non-volatile data processing and storage as well as processing-in-memory applications. By giving an overview of the current status of the field, we hope to facilitate progress on elucidating the different underlying physical mechanisms for the SOTs.

AUTHOR CONTRIBUTIONS

Both authors compiled the studies and wrote the manuscript.

ACKNOWLEDGMENTS

We acknowledge funding from the Dutch Research Council (NWO) Start-Up Grant (STU.019.014), the European Union Horizon 2020 research and innovation program under grant agreements No 696656 and 785219 (Graphene Flagship Core 2 and Core 3), and the Zernike Institute for Advanced Materials.

REFERENCES

Amin, V. P., Haney, P. M., and Stiles, M. D. (2020). Interfacial spin-orbit torques. arXiv: 2008.01182.

Amin, V. P., and Stiles, M. D. (2016a). Spin transport at interfaces with spin-orbit coupling: Formalism. *Phys. Rev. B* 94, 104419. doi:10.1103/PhysRevB.94.104419

Amin, V. P., and Stiles, M. D. (2016b). Spin transport at interfaces with spin-orbit coupling: Phenomenology. *Phys. Rev. B* 94, 104420. doi:10.1103/PhysRevB.94.104420

Avci, C. O., Garello, K., Gabureac, M., Ghosh, A., Fuhrer, A., Alvarado, S. F., et al. (2014). Interplay of spin-orbit torque and thermoelectric effects in ferromagnet/normal-metal bilayers. *Phys. Rev. B* 90, 224427. doi:10.1103/PhysRevB.90.224427

Berger, A. J., Edwards, E. R. J., Nembach, H. T., Karenowska, A. D., Weiler, M., and Silva, T. J. (2018). Inductive detection of fieldlike and dampinglike ac inverse spin-orbit torques in ferromagnet/normal-metal bilayers. *Phys. Rev. B* 97, 094407. doi:10.1103/PhysRevB.97.094407

Bonell, F., Goto, M., Sauthier, G., Sierra, J. F., Figueroa, A. I., Costache, M. V., et al. (2020). Control of spin-orbit torques by interface engineering in topological insulator heterostructures. *Nano Lett.* 20, 5893–5899. doi:10.1021/acs.nanolett.0c01850

Clark, O. J., Neat, M. J., Okawa, K., Bawden, L., Marković, I., Mazzola, F., et al. (2018). Fermiology and superconductivity of topological surface states in PdTe2. *Phys. Rev. Lett.* 120, 1–7. doi:10.1103/PhysRevLett.120.156401

Dieny, B., Prejbeanu, I. L., Garello, K., Gambardella, P., Freitas, P., Lehndorff, R., et al. (2019). Opportunities and challenges for spintronics in the microelectronic industry. arXiv:1908.10584.

Dolui, K., and Nikolic, B. K. (2020). Spin-orbit-proximitized ferromagnetic metal by monolayer transition metal dichalcogenide: atlas of spectral functions, spin textures and spin-orbit torques in Co/MoSe2, Co/WSe2 and Co/TaSe2 heterostructures. *Phys. Rev. Mater.* 4, 104007.

Dolui, K., Petrovic, M. D., Zollner, K., Plechac, P., Fabian, J., and Nikolic, B. K. (2019). First-principles theory of proximity spin-orbit torque on a two-dimensional magnet: current-driven antiferromagnet-to-ferromagnet reversible transition in bilayer CrI3. *Nano Lett.* 20, 2288.

Dyakonov, M. I., and Perel, V. I. (1971). Current-induced spin orientation of electrons in semiconductors. *Phys. Lett.* 35, 459–460. doi:10.1016/0375-9601(71)90196-4

Edelstein, V. M. (1990). Spin polarization of conduction electrons induced by electric current in two-dimensional asymmetric electron systems. *Solid State Commun.* 73, 233–235. doi:10.1016/0038-1098(90)90963-C

Fan, Y., Kou, X., Upadhyaya, P., Shao, Q., Pan, L., Lang, M., et al. (2016). Electric-field control of spin-orbit torque in a magnetically doped topological insulator. *Nat. Nanotechnol.* 11, 352–359. doi:10.1038/nnano.2015.294

Fang, D., Kurebayashi, H., Wunderlich, J., Výborný, K., Zârbo, L. P., Campion, R. P., et al. (2011). Spin-orbit-driven ferromagnetic resonance. *Nat. Nanotechnol.* 6, 413–417. doi:10.1038/nnano.2011.68

Filianina, M., Hanke, J.-P., Lee, K., Han, D.-S., Jaiswal, S., Rajan, A., et al. (2020). Electric-field control of spin-orbit torques in perpendicularly magnetized W/CoFeB/MgO films. *Phys. Rev. Lett.* 124, 217701. doi:10.1103/PhysRevLett.124.217701

Gambardella, P., and Miron, I. M. (2011). Current-induced spin-orbit torques. *Phil. Trans. R. Soc. A.* 369, 3175–3197. doi:10.1098/rsta.2010.0336

Ganichev, S. D., Ivchenko, E. L., Bel'kov, V. V., Tarasenko, S. A., Sollinger, M., Weiss, D., et al. (2002). Spin-galvanic effect. *Nature* 417, 153–156. doi:10.1038/417153a

Ganichev, S. D., Trushin, M., and Schliemann, J. (2016). Spin polarisation by current. *arXiv*.

Garello, K., Miron, I. M., Avci, C. O., Freimuth, F., Mokrousov, Y., Blügel, S., et al. (2013). Symmetry and magnitude of spin-orbit torques in ferromagnetic heterostructures. *Nat. Nanotechnol.* 8, 587–593. doi:10.1038/nnano.2013.145

Ghosh, A., Garello, K., Avci, C. O., Gabureac, M., and Gambardella, P. (2017). Interface-enhanced spin-orbit torques and current-induced magnetization switching of Pd/Co/AlOx layers. *Phys. Rev. Applied.* 7, 014004. doi:10.1103/PhysRevApplied.7.014004

Go, D., Freimuth, F., Hanke, J.-P., Xue, F., Gomonay, O., Lee, K.-J., et al. (2020). Theory of current-induced angular momentum transfer dynamics in spin-orbit coupled systems. *Phys. Rev. Res.* 2, 033401.

Go, D., and Lee, H.-W. (2020). Orbital torque: torque generation by orbital current injection. *Phys. Rev. Research.* 2, 013177. doi:10.1103/PhysRevResearch.2.013177

Guimarães, M. H. D., Stiehl, G. M., Macneill, D., Reynolds, N. D., Ralph, D. C., Guimaraes, M. H. D., et al. (2018). Spin-orbit torques in NbSe2/permalloy bilayers. *Nano Lett.* 18, 1311–1316. doi:10.1021/acs.nanolett.7b04993

Haney, P. M., Lee, H.-W., Lee, K.-J., Manchon, A., and Stiles, M. D. (2013). Current induced torques and interfacial spin-orbit coupling: semiclassical modeling. *Phys. Rev. B* 87, 174411. doi:10.1103/PhysRevB.87.174411

Hayashi, M., Kim, J., Yamanouchi, M., and Ohno, H. (2014). Quantitative characterization of the spin-orbit torque using harmonic Hall voltage measurements. *Phys. Rev. B* 89, 144425. doi:10.1103/PhysRevB.89.144425

Hirsch, J. E. (1999). Spin Hall effect. *Phys. Rev. Lett.* 83, 1834–1837. doi:10.1103/PhysRevLett.83.1834

Hoque, A. M., Khokhriakov, D., Karpiak, B., and Dash, S. P. (2020). Charge-spin conversion in layered semimetal TaTe2 and spin injection in van der Waals heterostructures. *Phys. Rev. Research.* 2, 033204. doi:10.1103/PhysRevResearch.2.033204

Husain, S., Chen, X., Gupta, R., Behera, N., Kumar, P., Edvinsson, T., et al. (2020). Damping-like torque in monolayer 1T-TaS2. aarXiv:2004.02649.

Kato, Y. K., Myers, R. C., Gossard, A. C., and Awschalom, D. D. (2004). Current-induced spin polarization in strained semiconductors. *Phys. Rev. Lett.* 93, 176601. doi:10.1103/PhysRevLett.93.176601

Kumar, A., Chaurasiya, A. K., Chowdhury, N., Mondal, A. K., Bansal, R., Barvat, A., et al. (2020). Direct measurement of interfacial Dzyaloshinskii-Moriya interaction at the MoS2/Ni80Fe20 interface. *Appl. Phys. Lett.* 116, 232405. doi:10.1063/5.0009828

Kurebayashi, H., Sinova, J., Fang, D., Irvine, A. C., Skinner, T. D., Wunderlich, J., et al. (2014). An antidamping spin-orbit torque originating from the Berry curvature. *Nat. Nanotechnol.* 9, 211–217. doi:10.1038/nnano.2014.15

Li, P., Wen, Y., He, X., Zhang, Q., Xia, C., Yu, Z.-M., et al. (2017). Evidence for topological type-II Weyl semimetal WTe2. *Nat. Commun.* 8, 2150. doi:10.1038/s41467-017-02237-1

Li, P., Wu, W., Wen, Y., Zhang, C., Zhang, J., Zhang, S., et al. (2018). Spin-momentum locking and spin-orbit torques in magnetic nano-heterojunctions composed of Weyl semimetal WTe2. *Nat. Commun.* 9, 1–10. doi:10.1038/s41467-018-06518-1

Li, X., Casamento, J., Dang, P., Zhang, Z., Afuye, O., Mei, A. B., et al. (2020). Spin-orbit torque field-effect transistor (SOTFET): proposal for a magnetoelectric memory. *Appl. Phys. Lett.* 116, 242405. doi:10.1063/5.0002909

Liu, L., Moriyama, T., Ralph, D. C., and Buhrman, R. A. (2011). Spin-torque ferromagnetic resonance induced by the spin Hall effect. *Phys. Rev. Lett.* 106, 036601. doi:10.1103/PhysRevLett.106.036601

Lv, W., Jia, Z., Wang, B., Lu, Y., Luo, X., Zhang, B., et al. (2018). Electric-field control of spin-orbit torques in WS2/permalloy bilayers. *ACS Appl. Mater. Interfaces.* 10, 2843–2849. doi:10.1021/acsami.7b16919

MacNeill, D., Stiehl, G. M., Guimaraes, M. H. D., Buhrman, R. A., Park, J., and Ralph, D. C. (2017a). Control of spin-orbit torques through crystal symmetry in WTe2/ferromagnet bilayers. *Nat. Phys.* 13, 300–305. doi:10.1038/nphys3933

MacNeill, D., Stiehl, G. M., Guimarães, M. H. D., Reynolds, N. D., Buhrman, R. A., and Ralph, D. C. (2017b). Thickness dependence of spin-orbit torques generated by WTe2. *Phys. Rev. B* 96, 1–8. doi:10.1103/PhysRevB.96.054450

Manchon, A., Železný, J., Miron, I. M., Jungwirth, T., Sinova, J., Thiaville, A., et al. (2019). Current-induced spin-orbit torques in ferromagnetic and antiferromagnetic systems. *Rev. Mod. Phys.* 91, 035004. doi:10.1103/RevModPhys.91.035004

Mellnik, A. R., Lee, J. S., Richardella, A., Grab, J. L., Mintun, P. J., Fischer, M. H., et al. (2014). Spin-transfer torque generated by a topological insulator. *Nature* 511, 449–451. doi:10.1038/nature13534

Mihai Miron, I., Gaudin, G., Auffret, S., Rodmacq, B., Schuhl, A., Pizzini, S., et al. (2010). Current-driven spin torque induced by the Rashba effect in a ferromagnetic metal layer. *Nat. Mater.* 9, 230–234. doi:10.1038/nmat2613

Miron, I. M., Garello, K., Gaudin, G., Zermatten, P.-J., Costache, M. V., Auffret, S., et al. (2011). Perpendicular switching of a single ferromagnetic layer induced by in-plane current injection. *Nature* 476, 189–193. doi:10.1038/nature10309

Nguyen, M.-H., Ralph, D. C., and Buhrman, R. A. (2016). Spin torque study of the spin Hall conductivity and spin diffusion length in platinum thin films with varying resistivity. *Phys. Rev. Lett.* 116, 126601. doi:10.1103/PhysRevLett.116.126601

Ramaswamy, R., Lee, J. M., Cai, K., and Yang, H. (2018). Recent advances in spin-orbit torques: moving towards device applications. *Appl. Phys. Rev.* 5, 031107. doi:10.1063/1.5041793

Safeer, C. K., Ontoso, N., Ingla-Aynés, J., Herling, F., Pham, V. T., Kurzmann, A., et al. (2019). Large multidirectional spin-to-charge conversion in low-symmetry semimetal MoTe2 at room temperature. *Nano Lett.* 19, 8758–8766. doi:10.1021/acs.nanolett.9b03485

Sahoo, K. R., Chakravarthy, T. P., Sharma, R., Bawari, S., Mundlia, S., Sasmal, S., et al. (2020). Probing proximity-tailored high spin-orbit coupling in 2D materials. *Adv Quantum Tech.* 3, 2000042. doi:10.1002/qute.202000042

Shao, Q., Yu, G., Lan, Y.-W., Shi, Y., Li, M.-Y., Zheng, C., et al. (2016). Strong rashba-edelstein effect-induced spin-orbit torques in monolayer transition metal dichalcogenide/ferromagnet bilayers. *Nano Lett.* 16, 7514–7520. doi:10.1021/acs.nanolett.6b03300

Shi, S., Liang, S., Zhu, Z., Cai, K., Pollard, S. D., Wang, Y., et al. (2019). All-electric magnetization switching and Dzyaloshinskii-Moriya interaction in WTe2/ferromagnet heterostructures. *Nat. Nanotechnol.* 14, 945–949. doi:10.1038/s41565-019-0525-8

Sinova, J., Valenzuela, S. O., Wunderlich, J., Back, C. H., and Jungwirth, T. (2015). Spin Hall effects. *Rev. Mod. Phys.* 87, 1213–1260. doi:10.1103/RevModPhys.87.1213

Sousa, F. J., Tatara, G., and Ferreira, A. (2020). Emergent spin-orbit torques in two-dimensional material/ferromagnet interfaces. arXiv:2005.09670.

Stiehl, G. M., Li, R., Gupta, V., Baggari, I. E., Jiang, S., Xie, H., et al. (2019a). Layer-dependent spin-orbit torques generated by the centrosymmetric transition metal dichalcogenide β–MoTe2. *Phys. Rev. B* 100, 184402. doi:10.1103/PhysRevB.100.184402

Stiehl, G. M., MacNeill, D., Sivadas, N., El Baggari, I., Guimarães, M. H. D., Reynolds, N. D., et al. (2019b). Current-induced torques with dresselhaus symmetry due to resistance anisotropy in 2D materials. *ACS Nano.* 13, 2599–2605. doi:10.1021/acsnano.8b09663

Wang, Y., Deorani, P., Banerjee, K., Koirala, N., Brahlek, M., Oh, S., et al. (2015). Topological surface states originated spin-orbit torques inBi2Se3. *Phys. Rev. Lett.* 114, 257202. doi:10.1103/PhysRevLett.114.257202

Wang, Y., Zhu, D., Wu, Y., Yang, Y., Yu, J., Ramaswamy, R., et al. (2017). Room temperature magnetization switching in topological insulator-ferromagnet heterostructures by spin-orbit torques. *Nat. Commun.* 8, 1364. doi:10.1038/s41467-017-01583-4

Wu, Y., Zhang, S., Zhang, J., Wang, W., Zhu, Y. L., Hu, J., et al. (2020). Néel-type skyrmion in WTe2/Fe3GeTe2 van der Waals heterostructure. *Nat. Commun.* 11, 3–8. doi:10.1038/s41467-020-17566-x

Xu, H., Wei, J., Zhou, H., Feng, J., Xu, T., Du, H., et al. (2020). High spin Hall conductivity in large-area type-II Dirac semimetal PtTe 2. *Adv. Mater.* 32, 2000513. doi:10.1002/adma.202000513

Xue, F., Rohmann, C., Li, J., Amin, V., and Haney, P. (2020). Unconventional spin-orbit torque in transition metal dichalcogenide -ferromagnet bilayers from first-principles calculations. *Phys. Rev. B* 102, 014401.

Zhang, W., Sklenar, J., Hsu, B., Jiang, W., Jungfleisch, M. B., Xiao, J., et al. (2016). Research Update: spin transfer torques in permalloy on monolayer MoS2. *Apl. Mater.* 4, 032302. doi:10.1063/1.4943076

Zhang, X., Liu, Q., Luo, J.-W., Freeman, A. J., and Zunger, A. (2014). Hidden spin polarization in inversion-symmetric bulk crystals. *Nat. Phys.* 10, 387–393. doi:10.1038/nphys2933

Zhao, B., Khokhriakov, D., Zhang, Y., Fu, H., Karpiak, B., Hoque, A. M., et al. (2020). Observation of charge to spin conversion in Weyl semimetal WTe2 at room temperature. *Phys. Rev. Research.* 2, 1–8. doi:10.1103/physrevresearch.2.013286

Zollner, K., Petrovic, M. D., Dolui, K., Plechac, P., Nikolic, B. K., and Fabian, J. (2020). Scattering-induced and highly tunable by gate damping-like spin-orbit torque in graphene doubly proximitized by two-dimensional magnet Cr2Ge2Te6 and monolayer WS2. *Phys. Rev. Res.* 2, 043057.

Conflict of Interest: The authors declare that the research was conducted in the absence of any commercial or financial relationships that could be construed as a potential conflict of interest.

Copyright © Hidding and Guimaraes. This is an open-access article distributed under the terms of the Creative Commons Attribution License (CC BY). The use, distribution or reproduction in other forums is permitted, provided the original author(s) and the copyright owner(s) are credited and that the original publication in this journal is cited, in accordance with accepted academic practice. No use, distribution or reproduction is permitted which does not comply with these terms.